PAPER

Catalytic performance of PVP-coated CuO nanosheets under environmentally friendly conditions†

Mahdi Shahmiri, [ID] *[a] Saadi Bayat [ID] [b] and Sharmin Kharrazi [ID] [a]

Aromatic nitro compounds are an increasing concern worldwide due to their potential toxicity, prompting a quest for efficient removal approaches. This study established a simple and environmentally friendly method to synthesize a highly efficient, recoverable and stable CuO nanosheets catalyst to overcome public health and environmental problems caused by nitro aromatic compounds. In the current research, the effect of different concentrations of copper nitrate on the size and shape of CuO nanostructures in the chemical synthesis was studied. The CuO nanosheets were characterized by X-ray diffraction (XRD), transmission electron microscopy (TEM), thermogravimetric analysis (TGA), Fourier transform infrared spectroscopy (FTIR) and ultraviolet-visible spectrophotometry. It was found that at concentrations of 0.07 M and 0.1 M of copper nitrate, pure CuO was formed. The FTIR results showed that carbonyl group in PVP coordinated with CuO and formed a protective layer. The as-synthesized CuO nanosheets with an average width of 60 ± 23 nm and length of 579 ± 154 were used as a catalyst for highly selective and efficient reduction of aromatic nitro and aromatic carboxylic acid to the corresponding amine and alcohol compounds. The reduction reaction was monitored by either UV-Vis absorption spectroscopy or high performance liquid chromatography (HPLC). 4-Nitrophenol and 4-nitroaniline were reduced to corresponding amine compounds within 12 min and 6 min, respectively in the presence of a reasonable amount of catalyst and reducing agent. The CuO nanosheets also exhibited excellent stability. The catalyst can be reused without loss of its activity after ten runs.

1. Introduction

Nitroaromatic compounds are extremely mutagenic and toxic and many of them are recognized as carcinogenic.[1–4] Their interactions with DNA, which result in mutagenicity, have been extensively examined and reviewed for a variety of heterocyclic, polycyclic, and monocyclic nitroaromatic compounds.[3] Consequently, the elimination of nitroaromatic compounds has always been an important concern especially, in wastewater treatment. Many efforts have been focused on the development of effective approaches to convert nitroaromatic to the corresponding amine compounds. Amines and their derivatives have a huge market share in the organic chemical sector.[5,6] For instance, 4-nitrophenol (4-NP) is a refractory organic pollutant, while, 4-aminophenol (4-AP) is used for the production of antipyretic and analgesic drugs such as acetanilide,

paracetamol, and phenacetin. Additionally, it is a very important ingredient in the production of industrial dyes, it is marketed as a photographic developer and its oxalate salt is used as a corrosion inhibitor.[7] Traditionally, the conversion of aromatic nitro compounds into aromatic amines is performed through metallic reagents (iron and tin) in acidic media.[8,9] But the major drawbacks of these methods include expensive nature, corrosion of the equipment, formation of large amounts of metal oxide sludge, *etc.*[10,11] Due to the need for some characteristics such as environmentally friendly, greener route, and safer operation direct catalytic conversion routes have been developed for the conversion of nitro compounds to amines.[12] One such route involves direct hydrogenation of nitro compounds using sodium borohydride (NaBH$_4$) which is a milder agent.[13] The reaction that is carried out in an aqueous medium, is relatively simple, and clean (eqn (1)).

$$NaBH_4(s) + 2H_2O \rightarrow 4H_2(g) + NaBO_2(aq) \tag{1}$$
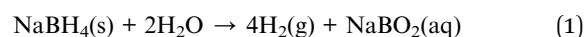
However, the sluggish self-hydrolysis of NaBH$_4$ affects the rate of hydrogenation of the nitro compound. The chemical reduction of the nitro group with NaBH$_4$ is extremely slow, and hence it is necessary to use a catalyst. A variety of catalysts such as gold,[14] silver,[15] Ni,[16] palladium,[17] RANEY® nickel,[18] and

[a]Department of Medical Nanotechnology, School of Advanced Technologies in Medicine (SATiM), Tehran University of Medical Sciences, Tehran, Iran. E-mail: mshahmiri@razi.tums.ac.ir

[b]Department of Chemistry and Physics, La Trobe Institute for Molecular Science, La Trobe University, Bundoora, Vic 3086, Australia

platinum[19] are used for the reduction of aromatic nitro into aromatic amines. However, costly metals including platinum and palladium, and RANEY® Ni are flammable along with the necessity of an inert atmosphere. Furthermore, catalytic reactions used in industrial applications to convert aromatic nitro compounds into aromatic amines, such as Ni sulfides, Pd/Al$_2$O$_3$, and Pd–Pt/C (Fe as modifier) need to be performed at elevated temperatures and pressures.[20]

Nanosized materials due to having specific properties such as highly acidic active sites and high surface area are ideal candidates to be used as catalysts.[21] Nanosized catalysts, such as faujasite NaY zeolite,[22] Mg–Fe hydrotalcite,[23] and polymer-supported Ni–B NPs[24] have been utilized for the hydrogenation of nitroarenes. The main disadvantages of these catalysts are that their activity decreases with consequent recycling and also their reactions are conducted under reflux, which requires several hours.[25] In recent years, transition metal oxides (TMOs) have attracted growing interest due to their particular physical and chemical properties such as chemical and thermal stability, high reactivity, and reusability.[26,27] One of the unique properties of TMOs is the large surface-to-volume ratio, which makes them prime candidates for catalysts. However, the small size and high surface energy of metal oxide nanoparticles often leads to agglomeration.[28,29] Therefore, polymers and surfactants are often used as capping agents to increase the stability of the metal oxide nanoparticles.[30] Among polymers, polyvinylpyrrolidone (PVP), is the most commonly used polymer in the preparation of metal oxide nanoparticles mainly because of its chemical stability, biocompatibility, low toxicity, and distinct shape.[30] Tu et al. synthesized several PVP-stabilized colloidal platinum metal nanoparticles and showed that PVP is a good stabilizer to protect Pt nanoparticles.[31] It has also been shown that the size of nanomaterials synthesized by PVP was dependent on the amount and type of PVP.[32] Among transition metal oxides, copper oxide (CuO) nanoparticles, due to their different technological applications such as catalysis,[33,34] antibacterial activity,[35] and CO oxidation[36] have gained much more attention. Compared to the catalysts of other transition metal oxides, CuO is comparatively cheaper, easily available, scalable, abundant, and has higher catalytic activity and simpler preparation. CuO is a transition metal oxide and a p-type semiconducting material with a monoclinic crystalline structure and cell parameters $a = 0.4684$ nm, $b = 0.3423$ nm, $c = 0.5128$ nm, and $\beta = 99.54°$.[37] Many different physical and chemical methods have been utilized to synthesize CuO nanoparticles.[38–41] The use of the quick precipitation method is particularly more attractive due to its cost effectiveness, simple operation, safe, and environmentally friendly procedure. The lack of study on CuO nanostructures for the reduction of nitrophenol has prompted researchers of the present study to investigate the catalytic activity of CuO nanostructures. In the present study, CuO nanosheets were synthesized under mild condition without using any support. For the determination of an appropriate synthesis condition, the concentration of CuNO$_3$ was changed in the reaction mixture. The catalytic behaviour of CuO nanosheets, that were good in terms of shape are studied for the reduction of aromatic nitro and aromatic carboxylic acid to the

corresponding amine and alcohol compounds in an aqueous medium using sodium borohydride (NaBH$_4$) as the reducing agent. The kinetics and mechanism have also been discussed.

2. Results and discussion

The XRD patterns of the products obtained with the variation of copper nitrate concentration (0.07 M, 0.1 M, and 0.14 M) at pH 10 are shown in Fig. 1. All the diffraction peaks of the samples obtained at 0.07 M and 0.1 M are attributed to the monoclinic phase of CuO with the lattice parameters matching with standard values. However, further increasing the concentration of copper nitrate to 0.14 M resulted in the diffraction peaks located at $2\theta = 12.80$, 25.79, and 33.48 (shown by asterisk) related to impurity phases.

The TEM micrographs of CuO samples prepared at concentrations of 0.1 M and 0.07 M (Fig. 2) revealed that particles have sheet-like geometry with an average width of 60 ± 23 nm and an average length of 579 ± 154 nm and a width of 204 ± 96 nm and a length of 548 ± 160 nm, respectively.

The results illustrated that variation in the concentration of Cu^{2+} has a remarkable effect on the size of final products. Wu et al. (2010)[41] investigated the effect of different molar ratios of Cu^{2+}/OH$^-$ on the size and shape of CuO nanoparticles. It has been shown that when the molar ratio was 1 : 4 rod-like particles were obtained, whereas when the molar ratio was 1 : 5 larger particles of the same shape were formed. They speculated that
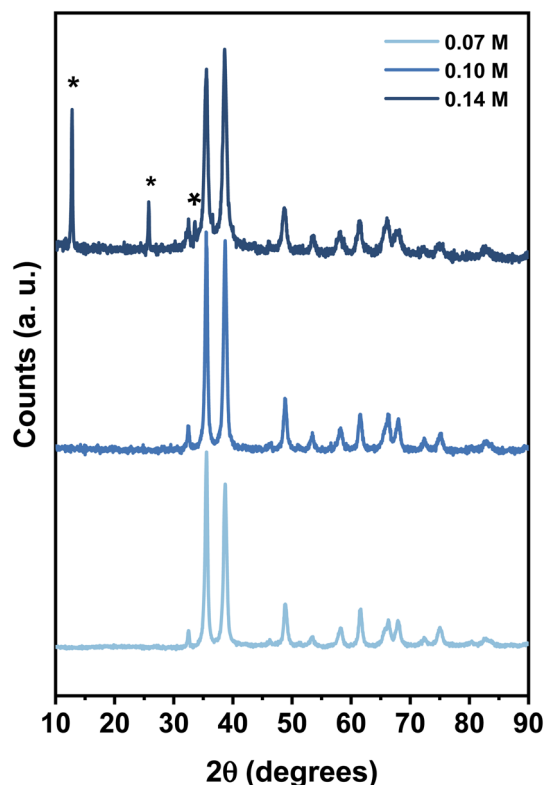

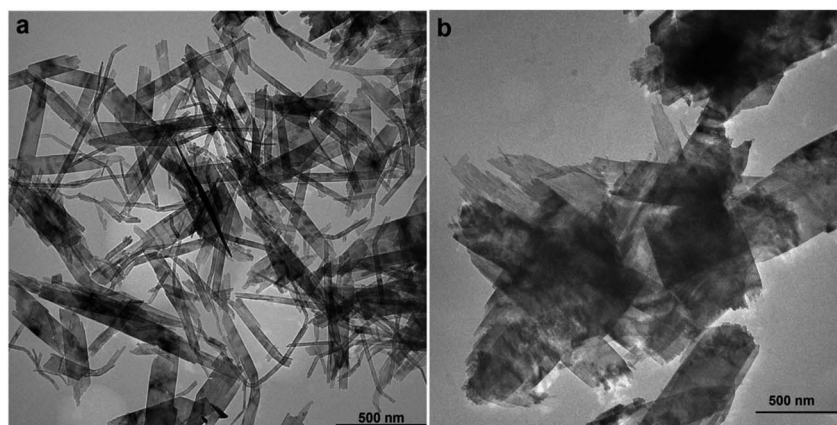Fig. 1 XRD pattern of the CuO samples prepared with different concentrations of Cu^{2+}.

Fig. 2 The TEM micrographs of CuO nanosheets prepared at 0.1 M (a) 0.07 M (b) concentration of Cu^{2+}.

forming larger particles could be related to the formation of H-bonds *via* interaction of OH^- ions, leading to aggregation. Therefore, it can be explained in this way that at 0.1 M required amount of OH^- reacted with Cu^{2+} to form CuO precipitates, then extra OH^- ions surrounded CuO precipitates and formed H-bonds through interconnection. It has been proposed that H-bonds could accelerate the rate of aggregation.[42] By decreasing the concentration of Cu^{2+} to 0.07 M, an excess amount of OH^- in the solution was present, which resulted in the formation of larger particles. To examine the effect of PVP on the size of the final product, the specimen was prepared at 1.5 wt% of PVP, while other variants were kept constant ($[Cu^{2+}] = 0.1$ M and pH $= 10$). TEM micrographs (Fig. S1†) revealed that particles have sheet-like geometry with a width of 160 ± 68 nm and length of 446 ± 127 nm.

The comparison between the particles obtained at 5 wt% and 1.5 wt% of PVP shows that by decreasing the concentration of PVP, the width of particles increased and their length decreased. This can be explained by the polymer selective adsorption.[43] It is considered that the existence of selective capping agents, such as PVP in a reaction could control the growth rates of various faces of metal oxide nanoparticles throughout the adsorption on these surfaces *via* Cu–N and Cu–O coordination bonds.[44] In the case of Ag nanocrystals DFT studies revealed that the surface–selective interaction of PVP with {111} and {100} facets occurs *via* direct binding and van der Waals attraction through oxygen atom.[45] It has also been shown that PVP strongly binds to {100} facet than {111}. Different shapes of gold nanostructures were synthesized using PVP as a shape-directing polymer. The authors suggested that PVP enhanced the growth rate along [100] directions and reduced the growth rate along [111] directions.[46] These results demonstrate that PVP interacts in a way completely different from Ag, stabilizing {100} facets, compared to {111} facets of Au.[46,47] In another study, Pt cubes and tetrahedral were synthesized using a PVP-assisted polyol process.[48,49] The results showed PVP functions similar to what is observed in the PVP-Ag system in which PVP is preferentially adsorbed onto the {100} facets.

Chen and co-workers synthesized TiO_2 nanosheets using PVP as a stabilizer.[50] They showed that PVP adsorbed on the facets caused hampering their growth. Xia *et al.* 2011 synthesized CuO chain-like hierarchically nanostructured using PVP (MW 30 000). SEM analysis of the sample showed the average size of CuO to be about 1 μm in diameter and several micrometers in length.[47] According to the aforementioned results, it is concluded that PVP as a selective polymer can
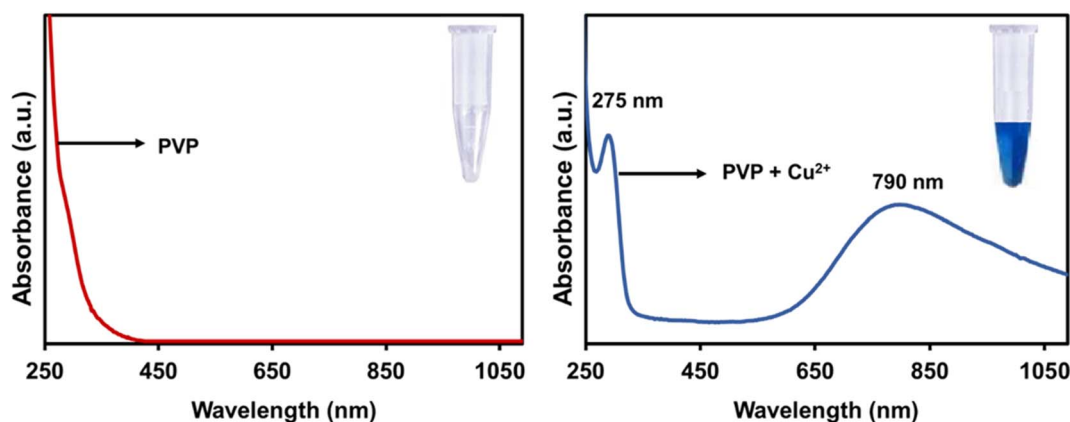

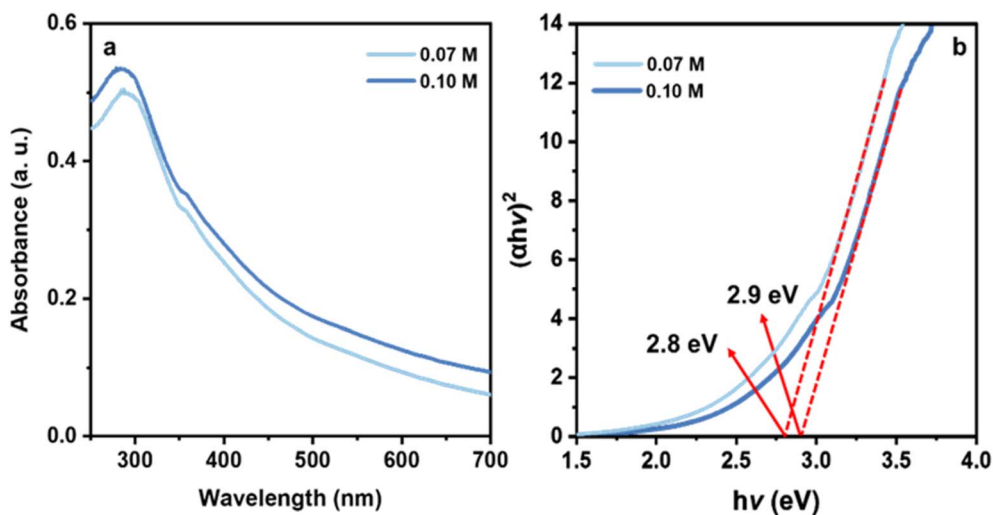Fig. 3 UV-Visible absorption spectra of PVP in the absence and present of Cu^{2+}.

Fig. 4 UV-Visible absorption spectra of CuO nanosheets obtained at 0.1 M and 0.07 M of Cu^{2+} (a), and their respective Tauc plot for determination of optical bandgap (b).

reduce growth rate along some specific crystal faces while promoting others. Therefore, we suggest that increasing the amount of PVP led to reducing the growth rate along the [100] directions and enhancing the growth rate along [010] directions. It should be noted that increasing the polymer concentration by more than 5% caused the system to become so viscous and it was difficult to collect the CuO nanosheets.

The UV-Vis absorption spectrum was used to investigate the optical properties of the CuO nanosheets. PVP has no absorption in the range of 200–800 nm (Fig. 3) but when trace amounts of Cu^{2+} ion was added to the colourless PVP solution, the colour
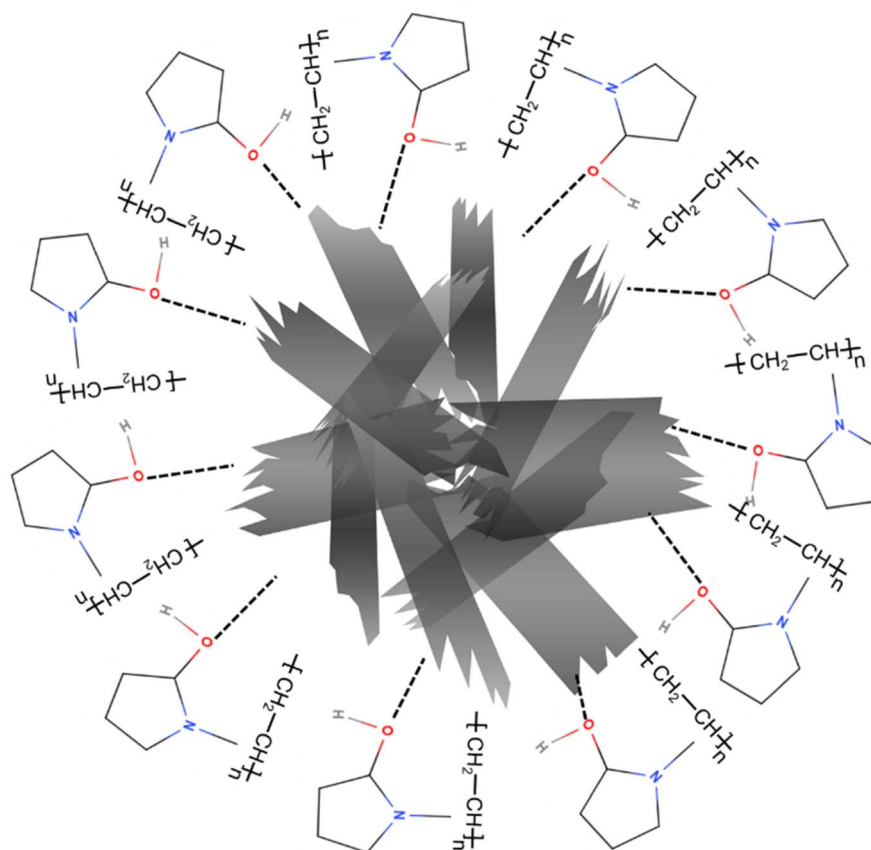

Fig. 5 Schematic diagram of the interaction of PVP chains with CuO nanosheets through H-bonding.
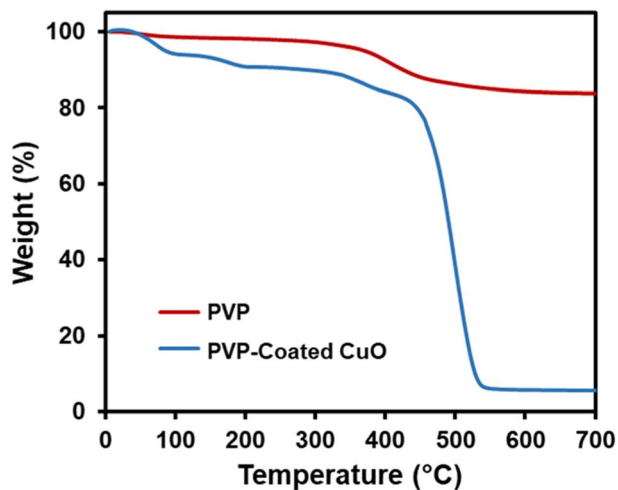
Fig. 6 TGA curve of the PVP-coated CuO nanosheets and pure PVP.

Fig. 7 FT-IR spectra of pure PVP, CuO synthesized without PVP (bulk) and PVP-coated CuO nanosheets.

of the mixture turned blue and displayed two absorption bands at 275 nm and 760 nm. The appearance of these two absorption bands is due to the formation of the Cu^{2+}/PVP complex since this process is a chromogenic response. Fig. 4(a) illustrates the UV-Visible absorption spectrum of the CuO nanosheets. The absorption peaks at 280, 287 nm are observed for the samples prepared at concentrations of 0.1 M and 0.07 M of Cu^{2+}, respectively. The spectra showed that the excitonic peak of the CuO nanosheets shifted to shorter wavelengths upon increasing the concentration of Cu^{2+} ions, which is in excellent agreement with the TEM results confirming the reduction in the size of nanosheets. It is therefore expected that these nanosheets exhibit a larger bandgap. Fig. 4(b) shows the Tauc plot and the respective optical band gap for CuO nanosheets obtained at 0.07 M and 0.1 M. The intersection between the linear fit and the energy axis gives the value to E_g. The corresponding calculated band gap energies are 2.8 eV for 0.07 M and 2.9 eV for 0.1 M. These two values are greater than the value for bulk CuO ($E_g = 1.2$ eV).[51]

It has been shown that PVP tends to be well-adsorbed onto the surface of metal oxide nanoparticles *via* H-bonding with an acid–base interaction[52] (Fig. 5). Therefore, thermogravimetric analysis was carried out to confirm whether the CuO was modified by PVP. Fig. 6 indicates four stages of weight loss observed for pure PVP. An initial weight loss observed in the range of room temperature to 106 °C was calculated to be 6.6%, which could be attributed to loss of moisture and loss of residual solvent. The second stage was 3.5% in the range of 106 °C to 181 °C. The third stage was 5.8% in the range of 243 °C to 330 °C. In the last stage that was 78.05%, a major weight loss began at 330 °C, which is attributed to the structural decomposition of the polymer. Fig. 6 also shows TGA analysis of PVP coated CuO nanosheets in which only one distinct stage of weight loss was observed at about 350 °C, which is attributed to the decomposition of the polymer. This result shows that the thermal stability of PVP is improved due to the presence of CuO nanostructures.
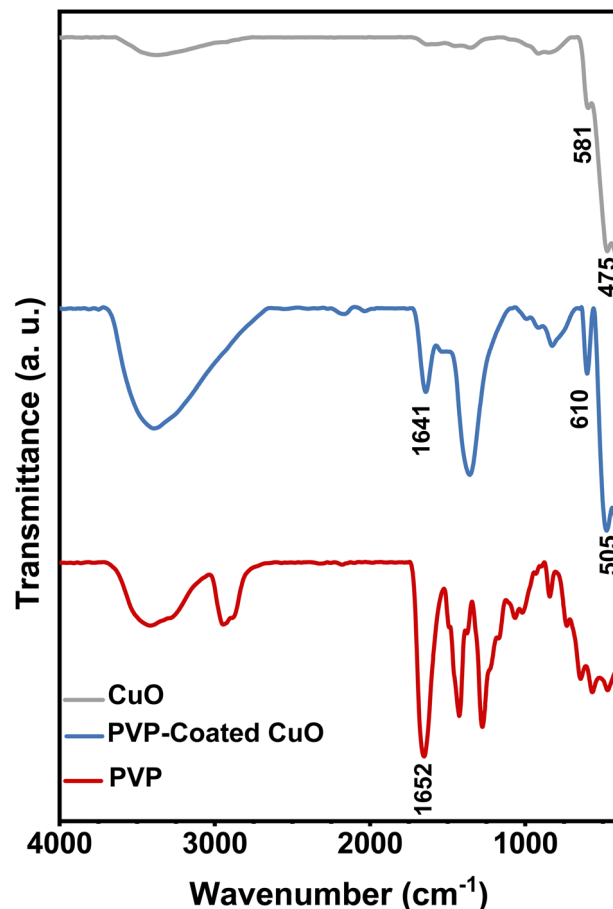
FTIR is a suitable and sensitive approach to detect the interaction between two species. In this study, FTIR was employed to confirm that the CuO nanostructures were modified by PVP. Fig. 7 demonstrates FT-IR spectra for pure PVP, bulk CuO and CuO/PVP nanosheets produced in PVP 5 wt%. In FT-IR spectrum of pure PVP, the peak at 1652 cm^{-1}, corresponds to the peak of C=O stretching vibration.[53] In the FTIR spectrum of PVP-coated CuO, the C=O stretching band is located at 1641 cm^{-1} compared to that for pure PVP. This red shift stems from the strong chemisorption of the C=O on the surface of CuO nanosheets that reduces the density of electrons in the carbonyl bond and therefore the vibratory energy.[54] Metal oxide commonly exhibits absorption bands below 1000 cm^{-1} arising from inter-atomic vibrations.[55,56] The absorption band at 475 cm^{-1} and 581 cm^{-1} in the FTIR spectrum of bulk CuO corresponds to Cu–O band stretching. Due to the interaction with PVP, these two peaks shifted to 505 cm^{-1} and 601 cm^{-1}, respectively. The presence of carbonyl peak that was absent in the bulk CuO spectrum indicates that PVP coordinated with CuO through carbonyl group and formed a protective layer.
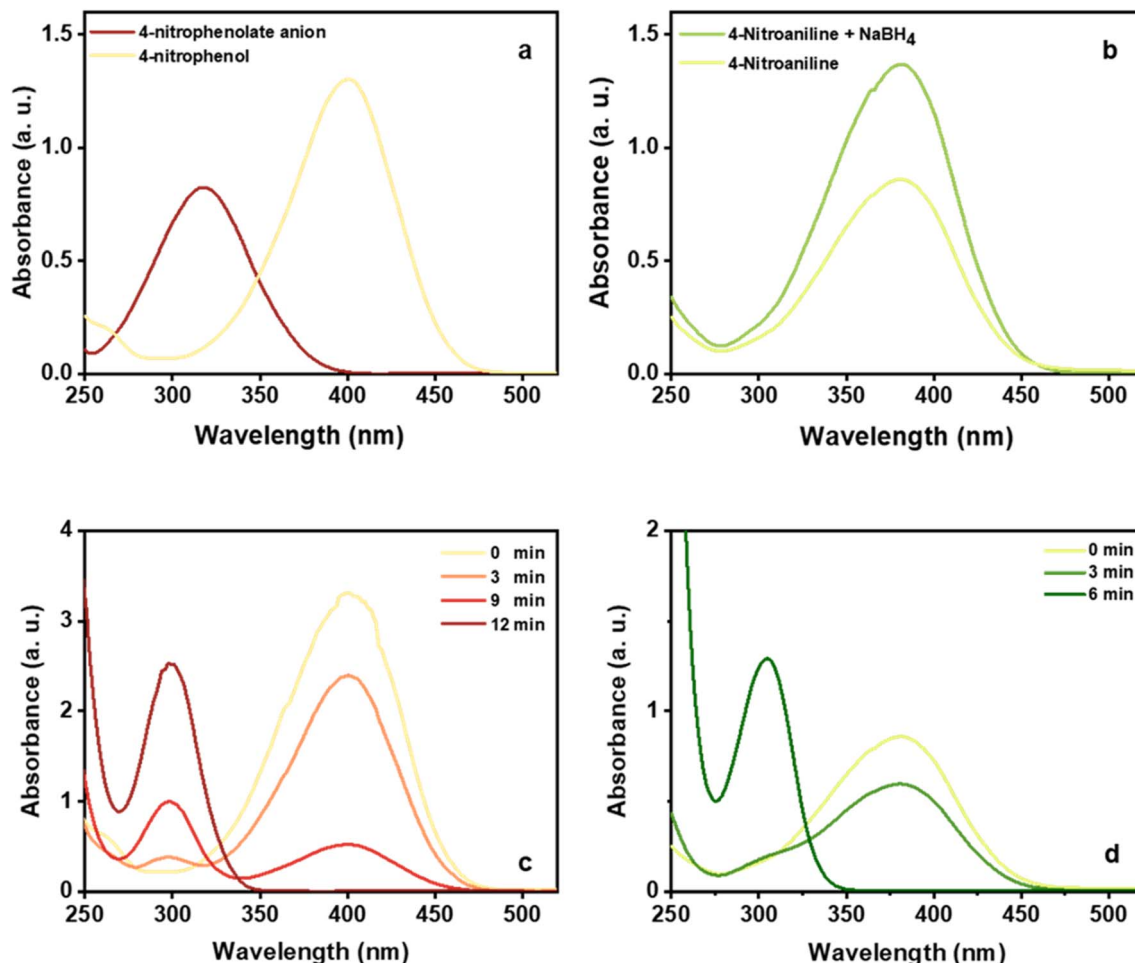
Fig. 8 UV–Vis absorption spectra for 4-NP and 4-NP + NaBH$_4$ (a) 4-NA and 4-NA + NaBH$_4$ (b) UV–4-NP + NaBH$_4$ + CuO (c) 4-NA + NaBH$_4$ + CuO (d).

2.1. Reduction of aromatic nitro group

Based on the above results, it was found that CuO nanosheets prepared at 0.1 M of Cu^{2+} are well-suited particles in terms of purity, size, and shape. As a result, this sample was chosen to study the catalytic activity of CuO nanosheets. The catalytic properties of CuO nanosheets were examined for NaBH$_4$ reduction of 4-NA and 4-NP in the presence and absence of the catalyst. The reduction process was monitored using UV-Visible spectroscopy. In addition, the yield and progress of reduction reactions were determined by HPLC (HPLC spectra of all the samples and products and be found in the supplementary data (Fig. S2–S22†). It was observed that after the addition of a freshly prepared ice-cold solution of NaBH$_4$, the peak of 4-NP was red-shifted from 321 to 401 nm due to the n$\rightarrow\pi^*$ transition (Fig. 8(a)). The colour of the reaction mixture was changed from pale yellow to deep yellow due to the formation of 4-nitrophenolate ion in an alkaline solution.[57] In the case of 4-NA, no shifting of the absorption peak at 382 nm was observed, however, the intensity of the peak increased after the addition of NaBH$_4$ (Fig. 8(b)) and the colour of the solution (yellow) remained unchanged for a couple of days without the addition

of CuO sheet-like particles. With the addition and proper mixing (stirring) of CuO nanosheets, the intensity of the peak at 401 nm gradually decreased, while a new peak at 300 nm appeared after 3 min and colour of the solution turned to brown, which substantiated the formation of 4-aminophenol (4-AP) Fig. 8(c).[58] The peak at 401 nm fully vanished after 12 min, suggesting the completion of the reduction reaction. In the case of 4-NA, the peak at 382 nm gradually decreased and a new peak started to appear at 308 nm after 3 min, due to the formation of 4-phenylenediamine.[59] The peak at 382 nm completely disappeared after 6 min (Fig. 8(d)). The reduction rate of 4-NA is

Table 1 Characteristic of CuO nanosheets at different concentrations of copper nitrate

Concentration of Cu^{2+} (M)	Concentration of PVP (wt%)	pH	Size (nm)	
			Width	Length
0.07	5	10	204 ± 96 nm	548 ± 160
0.1	5	10	60 ± 23 nm	579 ± 154
0.1	1.5	10	160 ± 68	446 ± 127

Table 2 Transfer reduction of aromatic nitro and carboxylic compounds to the corresponding amines and alcohols in the presence of CuO-nanosheets

Entry	Substrate	Product (final)	Time (min)	Yield [%] (HPLC)
1			12	100
2			12	100
3			15	100

Table 3 Reusability investigation of CuO nanosheets in reduction of 4-nitrophenol

Entry	Time (min)	Yield [%] (HPLC)
1	12	100
2	12	100
3	13	100
4	14	100
5	16	100
6	19	100
7	21	100
8	23	100
9	27	100
10	32	100

significantly higher than the reduction rate of 4-NP. It can be explained that the amine group in 4-NA is a donating group and provides a sufficient electron source for the nitro group in one hand, and proton on CuO sheet-like particles can absorb the oxygen of nitro easier.

With these findings in hand, we then extended our studies to reduce various kinds of aromatic nitro compounds and aromatic carboxylic acid to establish the scope of the CuO nanosheets. Table 2 exhibits that the catalyst system was surprisingly versatile. Various structurally diverse aryl nitro compounds and aromatic carboxylic acid could be selectively reduced to the corresponding amine and alcohol compounds. 4-Nitrobenzaldehyde, 2-nitrobenzaldehyde, and 5-amino-2-hydroxybenzoic acid (5-ASA) were reduced using $NaBH_4$ in the mixture of $MeOH : H_2O$ (1 : 1). In the first step, in the absence of catalyst, aldehyde group was reduced to alcohol (4 and 2-nitrobenzyl alcohol) and 5-ASA was remained intact during the reduction process. The reaction progress was monitored by HPLC (Fig. S2–S22†). In the absence of CuO-nanosheets $NaBH_4$ was capable of reducing only aldehyde group to alcohol. Whereas, with the addition of the CuO-nanosheets to the reaction, both nitro and carboxylic acid groups were converted to the corresponding products. Mandlimath et al.[60] studied catalytic activities of the first row transition metal oxides (TMOs) in the conversion of p-nitrophenol to p-aminophenol. The conversion happened at room temperature (30 °C) using aqueous $NaBH_4$. The results showed that CuO, Co, and NiO accelerated the reduction process. Conversely, the oxides such as TiO_2, V_2O_5, Cr_2O_3, MnO_2, and ZnO were found to be inactive towards the conversion of the p-nitrophenol. They argued that metal oxides having 'd^n' ($n = 5–9$) electronic configuration are

active catalysts because they relay electrons from the donor BH_4^- to the acceptor. They supposed that p-type semiconductors with a surface positive charge can facilitate the interaction between donor species BH_4^- and the surface of metal oxides.

2.2. Reusability of CuO nanosheets

The reusability of catalysts is a vital criterion for their practical applications. The reusability of the CuO nanosheets was tested by ten consecutive cycles and the results are shown in Table 3.

The catalyst was filtrated and employed without drying in the model reduction reaction of 4-nitrophenol to obtain the corresponding product. Interestingly, the catalyst was capable of reducing the nitro group to amine without a decrease in the yield of reaction (100% by HPLC), suggesting the excellent reusability of the catalyst. Although, the reaction time needed to full conversion of 4-nitrophenol increased from an initial 12 min to 32 min in the last run.

Mandlimath et al.[60] examined the reusability of CuO nanostructures. They showed that the conversion time decreased after the first run, suggesting the formation of metallic copper. The metallic copper catalyzed 4-NP at the same duration, showing that it is a highly effective catalyst even after tenth run. Conversely, in our case the conversion time increased after the first run, therefore, the formation of metallic copper can be ruled out. It was confirmed by XRD experiment (Fig. 9), which showed that the structure of CuO nanosheets was preserved after ten successive cycles. No trace of metallic Cu or Cu_2O_1 was observed.

To highlight the efficiency of the catalytic activity of CuO nanosheets, a comparison was made with catalysts reported in the literature (Table 4) in terms of the time needed to complete the reduction reaction of nitro compounds. It depicts that the reduction reaction is completed in a shorter time with an excellent yield using CuO nanosheets. It is worthwhile to note that some reports show that the reduction reaction of nitro compounds is done in a much shorter time compared to our work but with a very high amount of catalyst and reducing agent or a tiny amount of nitro compounds used. In the current research, the reduction reaction was carried out using 60 mg of nitro compounds dissolved in 3 ml DI water in the presence of

Table 4 List of various catalysts used for the reduction of aromatic nitro compounds

Particles	Reduction condition	Reduction time, yield	Ref.
CuO	4-Nitrophenol	16 min	60
NiO NPs	High temperature 4-nitrophenol	60 min, 96%	25
Ni NPs	*p*-Nitrophenol	25 min	10
Cu NPs	4-NP	45 to >100 min, 100%	66
Cu NPs CuBr$_2$ as pre-catalyst, which was *in situ* reduced to copper NPs	Nitrobenzene	300 min, 100%	67
Gum acacia-silica hybrid anchored Cu NPs	4-NP	2.3 min	61
Fe$_3$O$_4$ supported Cu-MOF	1,4-Dinitrobenzene	180 min, 95%	68
Fe–Ni NPs	4-Nitrophenol	180 min	69
Nickel loaded on TiO$_2$		30 min	
Ni–B/Al$_2$O$_3$	4-Nitrophenol	85 min, 96%	70
Fe$_3$O$_4$/β-alanine-acrylamide-Ni	Nine different nitroarenes	15 min	71
Spindly CuO micro-particles	4-Nitrophenol	90 min	72
CuO nanosheets	4-Nitrophenol	12 min, 100%	This work
CuO nanosheets	4-Nitroaniline	6 min, 100%	This work

120 mg (3.17 mmol) NaBH$_4$ and 4 mg CuO nanosheets in 2 ml DI water. Singh *et al.*[61] synthesized gum acacia-silica hybrid anchored Cu NPs and studied the reduction reaction of 4-NP. It was shown that the reduction completed within 2.3 min if 0.004 mg of 4-NP, 100 mM NaBH$_4$, and 3 mg catalyst were used. However, upon increasing the concentration of NaBH$_4$ to >0.1 M the reaction completed immediately. As can be seen a very little amount of 4-NP was used in this work. In another report, it was shown that if 0.8 mg CuO catalyst was used the reduction completed within 16 min but upon increasing the concentration of CuO catalyst to 100 mg the reduction time decreased to 40 seconds.[60] Furthermore, another advantage of the as-prepared CuO nanosheets is that our catalyst can reduce nitro and carboxyl compounds simultaneously. 4-Nitrobenzaldehyde,

2-nitrobenzaldehyde reduced to 4-aminobenzyl alcohol and 2-aminobenzyl alcohol respectively within 12 min. 5-Amino-2-hydroxybenzoic acid reduced to 4-amino-2-(hydroxymethyl) phenol within 15 min.

2.3. Mechanism

The mechanism of the hydrogenation of the nitro compound designates that the process is affected by the factors such as proton availability and electron transfer to the nitro compound.[62] There are two steps involved in this reaction: (a) CuO nanosheets react with borohydride ions to form the metal hydride on the surface of CuO nanosheets and (b) discharge of electrons from BH$_4^-$ through the metal oxide to the acceptor. Water is a polar protic solvent, and it supplies the required hydrogen ion for the completion of the reduction reaction.[63,64] The adsorption process plays an important role in catalysis. In this study, the CuO nanosheets catalyst provided the adsorption site for BH$_4^-$ ions as well as for the nitro aromatic compounds and also facilitated the transfer of electrons from the donor BH$_4^-$ ions to the nitro aromatic compound (acceptor) as depicted in Fig. 10.
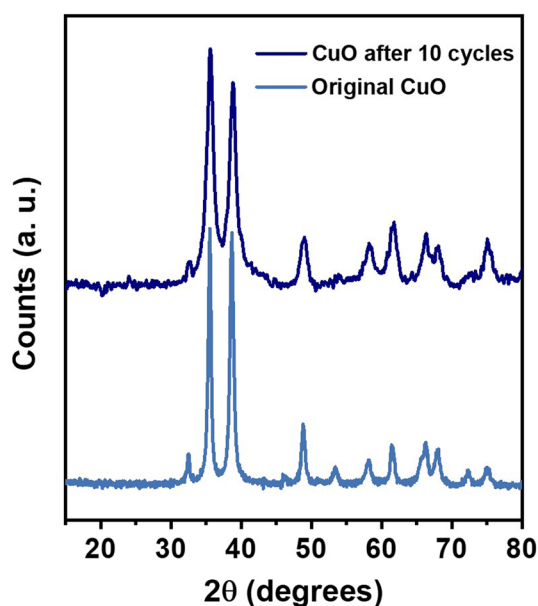
3. Conclusions

The CuO nanosheets were successfully synthesized at different concentrations of Cu^{2+} at pH = 10.00, using the quick precipitation method as a cost-effective, simple, safe, and environmentally friendly method. The results showed that PVP-coated CuO nanosheets exhibit excellent catalytic activity for the reduction of aromatic nitro and carboxylic group by NaBH$_4$ at room temperature. One of the most important features of CuO nanosheets catalyst is that it maintains an excellent activity and yield over ten runs. The current research is valuable in the development of CuO recoverable nanocatalyst, which is a highly efficient and stable catalyst to promote the reduction of nitro and carboxylic groups. These characteristics indicate the practical applications of CuO nanosheets in environmental remediation.
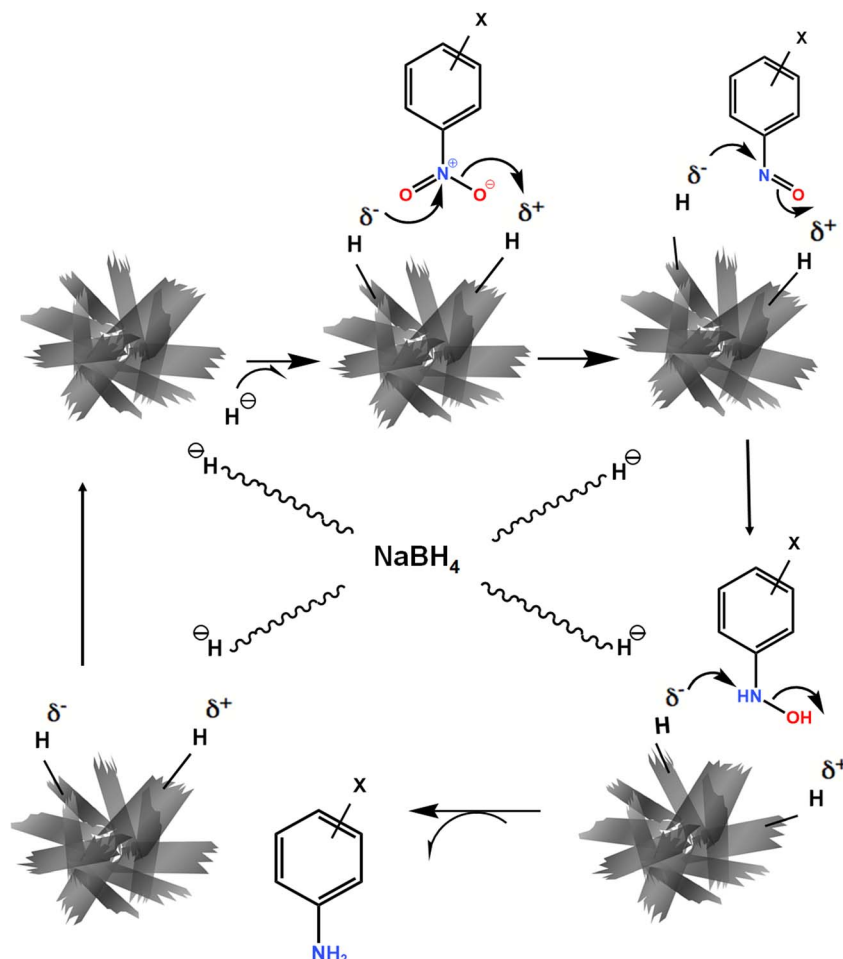

Fig. 9 The XRD patterns of the original CuO nanosheets and the CuO nanosheets recovered after 10 catalytic cycles.

Fig. 10 Schematic diagram of the proposed mechanism of nitro group reduction catalyzed by CuO nanosheets.

4. Experimental

4.1. Materials and methods

All the chemicals used were of analytical reagent grade and were used without any further purification. PVP (MW 10 000) was provided by Sigma-Aldrich (USA). Copper nitrate trihydrate (98%, $Cu(NO_3)_2 \cdot 3H_2O$) and sodium hydroxide (99.5%, NaOH) granules were purchased from Merck (Germany). 4-Nitrophenol (4-NP), 4-nitroaniline (4-NA) 4-nitrobenzaldehyde, 2-nitro-benzaldehyde, and 5-amino-2-hydroxybenzoic acid (5-ASA) were purchased from Sigma Aldrich (Germany).

4.2. Synthesis of CuO nanosheets

Different concentrations of $Cu(NO_3)_2 \cdot 3H_2O$ (Table 1) were dissolved in 60 ml aqueous solution of PVP 5% (w/v). The pH of the solutions was adjusted to 10 by adding NaOH (1 M) and the solutions were then maintained at 60 °C under stirring for 1 h until a large amount of black precipitates was achieved. Then the solutions were cooled down to room temperature, the black precipitate was separated by centrifugation, washed with deionized (DI) water, and then dried in an oven at 60 °C overnight.

4.3. Characterization

The structural analysis of the CuO nanostructures was done by X-ray diffraction using a PW1730/10 X-ray diffractometer (Ni filtered CuKα radiation, $\lambda = 1.542$ Å, Philips, The Netherlands). The size and shape of the final products were examined by transmission electron microscopy (TEM) using Philips-CM120 (Netherlands) operated at 100 kV. The specimens for TEM imaging were prepared by suspending solid samples in DI water. 1 mg of each powder was added to 5 ml DI water and was then sonicated at 35 kHz for 10 min. One drop of each solution was deposited on the copper grid and dried at 60 °C. The particle sizes were determined using UTHSCSA Image Tool version 3.00. The optical properties of CuO nanostructures were examined by UV-Vis spectrophotometer (Bio Aquarius CE 7250, United Kingdom). The yield and progress of reduction reactions were determined by HPLC (Waters 1525 Binary Pump and UV-Water 2489) analysis employing a reverse phase column (xbridge, 4.6 mm × 250 mm). Flow rate, 1 ml min⁻¹, mobile phase: ACN, in 220 nm. The compositions of the products were characterized by using the FT-IR spectroscopy. FTIR measurements can confirm chemical structure of nanoparticles and also can prove the modification of CuO NPs by PVP. FTIR spectra were recorded at ambient temperature using attenuated total

reflection (ATR) technique. The samples were scanned at a wavelength range of 400–4000 cm^{-1}, resolution of 4 cm^{-1}. The infrared spectra of samples were measured with a Thermo Nicolet Avatar 360 FTIR spectrometer. Thermogravimetric analysis (TGA) was carried out using on the pure PVP and CuO/PVP using (TA Instruments, SDT Q600, USA). Appropriate amount of samples was heated at a rate of 20 °C min^{-1} from room temperature up to 700 °C in flowing N$_2$.

4.4. Optical bandgap determination

The band gap is an important feature of semiconductors, which determines their applications in optoelectronics. The band gap indicated the difference in energy between the top of the valence band filled with electrons and the bottom of the conduction band devoid of electrons. The absorption spectra could be utilized to calculate the energy gap of the CuO nanosheets using Tauc's equation (eqn (2)).[65]

$$(\alpha h v)^n = B(h v - E_g) \qquad (2)$$

where h is Plank's constant, B is a constant related to the material, v is the photon's frequency, hv is the energy of the photon, n is an exponent that can be either 1/2 for an indirect transition or 2 for a direct transition, E_g is the optical bandgap, α is the absorption coefficient calculated through $\alpha d = \ln(1/T)$, where T is transmittance, and d is the path length of the wave. Using Tauc's equation, $\alpha h v$ was plotted against hv. A line is drawn tangent to the point of inflection on the curve and the hv value at the point of the intersection of the tangent line is the band gap value.

4.5. Catalytic performance test

4-NP and 4-NA (60 mg, 0.43 mmol) were dissolved in 3 ml distilled water and then NaBH$_4$ (120 mg, 3.17 mmol) was added. CuO nanosheets solution (4 mg in 2 ml DI water) was sonicated at 35 kHz for 10 minutes to homogenously disperse the particles then the catalyst solution was added to the above solution under vigorous stirring at room temperature. To dissolve 4-NP faster, 1 ml iso-propanol was added. The conversion of 4-NP and 4-NA nitro compounds were monitored by UV-Vis absorption spectroscopy.

4.6. Recycling of the catalyst

At the end of the reduction of 4-nitrophenol, the catalyst was filtered and employed in the model reduction reaction without drying. The results for ten runs are summarized in Table 3.

Conflicts of interest

The authors declare that there is no conflicts of interest.

Acknowledgements

References

1 G. I. Sunahara, G. Lotufo, R. G. Kuperman and J. Hawari, *Ecotoxicology of explosives*, CRC Press, 2009.

2 R. S. Padda, C. Wang, J. B. Hughes, R. Kutty and G. N. Bennett, *Environ. Toxicol. Chem.*, 2003, **22**, 2293–2297.

3 V. Purohit and A. K. Basu, *Chem. Res. Toxicol.*, 2000, **13**, 673–692.

4 P.-G. Rieger and H.-J. Knackmuss, in *Biodegradation of nitroaromatic compounds*, Springer, 1995, pp. 1–18.

5 P. F. Vogt and J. J. Gerulis, *Ullmann's Encyclopedia of Industrial Chemistry*, Wiley-VCH Verlag GmbH & Co. KGaA, Weinheim, Germany, 2000.

6 P. Roose, K. Eller, E. Henkes, R. Rossbacher and H. Höke, *Ullmann's Encyclopedia of Industrial Chemistry*, Wiley-VCH Verlag GmbH & Co. KGaA, Weinheim, Germany, 2000.

7 J. I. Kroschwitz, M. Howe-Grant, R. E. Kirk and D. F. Othmer, *Encyclopedia of chemical technology*, John Wiley & Sons, 1996.

8 C. A. Merlic, S. Motamed and B. Quinn, *J. Org. Chem.*, 1995, **60**, 3365–3369.

9 K. M. Doxsee, M. Feigel, K. D. Stewart, J. W. Canary, C. B. Knobler and D. J. Cram, *J. Am. Chem. Soc.*, 1987, **109**, 3098–3107.

10 Y. Du, H. Chen, R. Chen and N. Xu, *Appl. Catal., A*, 2004, **277**, 259–264.

11 M. J. Vaidya, S. M. Kulkarni and R. V. Chaudhari, *Org. Process Res. Dev.*, 2003, **7**, 202–208.

12 P. Liu and M. Zhao, *Appl. Surf. Sci.*, 2009, **255**, 3989–3993.

13 Y. Kojima, K.-i. Suzuki, K. Fukumoto, M. Sasaki, T. Yamamoto, Y. Kawai and H. Hayashi, *Int. J. Hydrogen Energy*, 2002, **27**, 1029–1034.

14 K. Kuroda, T. Ishida and M. Haruta, *J. Mol. Catal. A: Chem.*, 2009, **298**, 7–11.

15 J. N. Solanki and Z. V. P. Murthy, *Ind. Eng. Chem. Res.*, 2011, **50**, 7338–7344.

16 M. Blosi, S. Albonetti, A. Costa, N. Sangiorgi and A. Sanson, *Chem. Eng. J.*, 2013, **215**, 616–625.

17 S.-D. Oh, M.-R. Kim, S.-H. Choi, J.-H. Chun, K.-P. Lee, A. Gopalan, C.-G. Hwang, K. Sang-Ho and O. J. Hoon, *J. Ind. Eng. Chem.*, 2008, **14**, 687–692.

18 I. Pogorelić, M. Filipan-Litvić, S. Merkaš, G. Ljubić, I. Cepanec and M. Litvić, *J. Mol. Catal. A: Chem.*, 2007, **274**, 202–207.

19 D. C. Gowda and B. Mahesh, *Synth. Commun.*, 2000, **30**, 3639–3644.

20 D. Formenti, F. Ferretti, F. K. Scharnagl and M. Beller, *Chem. Rev.*, 2019, **119**, 2611–2680.

21 X. Cai, Z. Xie, D. Li, M. Kassymova, S.-Q. Zang and H.-L. Jiang, *Coord. Chem. Rev.*, 2020, **417**, 213366.

22 M. Kumarraja and K. Pitchumani, *Appl. Catal., A*, 2004, **265**, 135–139.

23 P. S. Kumbhar, J. Sanchez-Valente, J. M. M. Millet and F. Figueras, *J. Catal.*, 2000, **191**, 467–473.

24 H. Wen, K. Yao, Y. Zhang, Z. Zhou and A. Kirschning, *Catal. Commun.*, 2009, **10**, 1207–1211.

25 S. Farhadi and F. Siadatnasab, *J. Mol. Catal. A: Chem.*, 2011, **339**, 108–116.

26 G. Schmid, *Nanoparticles: from theory to application*, John Wiley & Sons, 2011.

27 S. Han, R. Raja, G. A. Somorjai and B. Zhou, *Nanotechnology in Catalysis*, Springer, 2007.

28 D. Lin and B. Xing, *Environ. Pollut.*, 2007, **150**, 243–250.

29 L. Yang and D. J. Watts, *Toxicol. Lett.*, 2005, **158**, 122–132.

30 R. Javed, M. Zia, S. Naz, S. O. Aisida and Q. Ao, *J. Nanobiotechnol.*, 2020, **18**, 1–15.

31 W. Tu, X. Zuo and H. Liu, *Chin. J. Polym. Sci.*, 2008, **26**, 23–29.

32 S. M. Briffa, I. Lynch, V. Trouillet, M. Bruns, D. Hapiuk, J. Liu, R. Palmer and E. Valsami-Jones, *RSC Adv.*, 2017, **7**, 3894–3906.

33 Z. Zhang, H. Che, Y. Wang, L. Song, Z. Zhong and F. Su, *Catal. Sci. Technol.*, 2012, **2**, 1953–1960.

34 R. Poreddy, C. Engelbrekt and A. Riisager, *Catal. Sci. Technol.*, 2015, **5**, 2467–2477.

35 D. Vinu, K. Govindaraju, R. Vasantharaja, S. Amreen Nisa, M. Kannan and K. Vijai Anand, *J. Nanostruct. Chem.*, 2021, **11**, 271–286.

36 H. Li, F.-X. Tian, Q. Liu, Y. Han and M. Zhu, *Catal. Sci. Technol.*, 2022, **12**, 6590–6598.

37 J. Jun, C. Jin, H. Kim, S. Park and C. Lee, *Appl. Surf. Sci.*, 2009, **255**, 8544–8550.

38 M. Kaur, K. Muthe, S. Despande, S. Choudhury, J. Singh, N. Verma, S. Gupta and J. Yakhmi, *J. Cryst. Growth*, 2006, **289**, 670–675.

39 M. A. Dar, Y. S. Kim, W. B. Kim, J. M. Sohn and H. S. Shin, *Appl. Surf. Sci.*, 2008, **254**, 7477–7481.

40 Z. Zhang and P. Wang, *J. Mater. Chem.*, 2012, **22**, 2456–2464.

41 R. Wu, Z. Ma, Z. Gu and Y. Yang, *J. Alloys Compd.*, 2010, **504**, 45–49.

42 W. Zhang, X. Wen and S. Yang, *Inorg. Chem.*, 2003, **42**, 5005–5014.

43 H. T. Zhu, C. Y. Zhang, Y. M. Tang and J. X. Wang, *J. Phys. Chem. C*, 2007, **111**, 1646–1650.

44 D. Volanti, D. Keyson, L. Cavalcante, A. Z. Simões, M. Joya, E. Longo, J. A. Varela, P. Pizani and A. Souza, *J. Alloys Compd.*, 2008, **459**, 537–542.

45 W. Al-Saidi, H. Feng and K. A. Fichthorn, *Nano Lett.*, 2012, **12**, 997–1001.

46 F. Kim, S. Connor, H. Song, T. Kuykendall and P. Yang, *Angew. Chem., Int. Ed.*, 2004, **43**, 3615.

47 X. Xia, J. Zeng, L. K. Oetjen, Q. Li and Y. Xia, *J. Am. Chem. Soc.*, 2012, **134**, 1793–1801.

48 S. Kweskin, R. Rioux, H. Song, K. Komvopoulos, P. Yang and G. Somorjai, *ACS Catal.*, 2012, **2**, 2377–2386.

49 H. Song, F. Kim, S. Connor, G. A. Somorjai and P. Yang, *J. Phys. Chem. B*, 2005, **109**, 188–193.

50 J. S. Chen, J. Liu, S. Z. Qiao, R. Xu and X. W. D. Lou, *Chem. Commun.*, 2011, **47**, 10443–10445.

51 P. Majumder and R. Gangopadhyay, *RSC Adv.*, 2022, **12**, 5686–5719.

52 J. Ryu, H.-S. Kim and H. T. Hahn, *J. Electron. Mater.*, 2011, **40**, 42–50.

53 W.-x. Tu, X.-b. Zuo and H.-f. Liu, *Chin. J. Polym. Sci.*, 2008, **26**, 23–29.

54 I. Safo, M. Werheid, C. Dosche and M. Oezaslan, *Nanoscale Adv.*, 2019, **1**, 3095–3106.

55 S. Shyamala and R. Muthuchudarkodi, *Int. J. Sci. Eng. Manag.*, 2018, **3**, 588–595.

56 P. L. Chaudhari and P. C. Kale, *Int. J. ChemTech Res.*, 2017, **10**, 477–486.

57 Y. Shi, X. Zhang, Y. Zhu, H. Tan, X. Chen and Z.-H. Lu, *RSC Adv.*, 2016, **6**, 47966–47973.

58 C. Tamuly, I. Saikia, M. Hazarika and M. R. Das, *RSC Adv.*, 2014, **4**, 53229–53236.

59 T. Aditya, A. Pal and T. Pal, *Chem. Commun.*, 2015, **51**, 9410–9431.

60 T. R. Mandlimath and B. Gopal, *J. Mol. Catal. A: Chem.*, 2011, **350**, 9–15.

61 V. Singh, A. Pandey, J. Singh and T. Malviya, *RSC Adv.*, 2016, **6**, 31074–31082.

62 K. Kuroda, T. Ishida and M. Haruta, *J. Mol. Catal. A: Chem.*, 2009, **298**, 7–11.

63 M. Blosi, S. Albonetti, A. Costa, N. Sangiorgi and A. Sanson, *Chem. Eng. J.*, 2013, **215**, 616–625.

64 J.-R. Chiou, B.-H. Lai, K.-C. Hsu and D.-H. Chen, *J. Hazard. Mater.*, 2013, **248**, 394–400.

65 J. Tauc, *Mater. Res. Bull.*, 1968, **3**, 37–46.

66 P. Deka, R. C. Deka and P. Bharali, *New J. Chem.*, 2014, **38**, 1789–1793.

67 H. K. Kadam and S. G. Tilve, *RSC Adv.*, 2012, **2**, 6057–6060.

68 S. Yang, Z. H. Zhang, Q. Chen, M. Y. He and L. Wang, *Appl. Organomet. Chem.*, 2018, **32**, e4132.

69 D. R. Petkar, B. S. Kadu and R. C. Chikate, *RSC Adv.*, 2014, **4**, 8004–8010.

70 H. Liu, J. Deng and W. Li, *Catal. Lett.*, 2010, **137**, 261–266.

71 F. Zamani and S. Kianpour, *Catal. Commun.*, 2014, **45**, 1–6.

72 J. Li, F. Sun, K. Gu, T. Wu, W. Zhai, W. Li and S. Huang, *Appl. Catal., A*, 2011, **406**, 51–58.